Insights into Redox Partner Interactions and Substrate Binding in Nitrite Reductase from *Alcaligenes xylosoxidans*: Crystal Structures of the Trp138His and His313Gln Mutants[†,‡]

Mark L. Barrett,[§,||] Roger L. Harris,[⊥] Svetlana Antonyuk,[||] Michael A. Hough,[||] Mark J. Ellis,[||] Gary Sawers,[#] Robert R. Eady,[⊥,||] and S. Samar Hasnain*[,§,||]

Faculty of Applied Sciences, De Montfort University, The Gateway, Leicester, LE1 9BH, United Kingdom, Molecular Biophysics Group, CCLRC Daresbury Laboratory, Warrington, WA4 4AD, United Kingdom, Biological Chemistry Department, John Innes Centre, Norwich NR4 7UH, United Kingdom, and Molecular Microbiology Department, John Innes Centre, Norwich, NR4 7UH, United Kingdom

Received June 24, 2004; Revised Manuscript Received October 4, 2004

ABSTRACT: Dissimilatory nitrite reductase catalyses the reduction of nitrite to nitric oxide within the key biological process of denitrification. We present biochemical and structural results on two key mutants, one postulated to be important for the interaction with the partner protein and the other for substrate entry. Trp138, adjacent to one of the type-1 Cu ligands, is one of the residues surrounding a small depression speculated to be important in complex formation with the physiological redox partners, azurin I and II. Our data reveal that the Trp138His mutant is fully active using methyl viologen as an artificial electron donor, but there is a large decrease in activity using azurin I. These observations together with its crystal structure at a high resolution of 1.6 Å confirm the importance of Trp138 in electron transfer and thus in productive interaction with azurin. A "hydrophobic pocket" on the protein surface has been identified as the channel through which nitrite may be guided to the catalytic type-2 Cu site. Glu133 and His313 at the opening of the pocket are conserved among most blue and green copper nitrite reductases (CuNiRs). The failure to soak the substrate into our high-resolution crystal form of native and mutant CuNiRs has been linked to the observation of an extraneous poly(ethylene glycol) (PEG) molecule interacting with His313. We present the crystal structure of His313Gln and the substrate-bound mutant at high resolutions of 1.65 and 1.72 Å, respectively. The observation of the substrate-bound structure for the His313Gln mutant and inhibitory studies with PEG establishes the role of the hydrophobic pocket as the port of substrate entry.

Nitrogen is introduced into the biosphere by the biological and chemical fixation of dinitrogen (N_2) and removed by the process of denitrification. Denitrification is an anaerobic respiratory pathway by which some bacteria carry out the sequential reduction of nitrate via nitrite, NO and N_2O to dinitrogen. Dissimilatory nitrite reductase (NiR)[1] is a key enzyme in this pathway, because it catalyses the first committed step of denitrification that leads to the gaseous product NO (*1*).

Two different classes of NiR are found in denitrifying bacteria, the haem and the Cu enzymes. Copper nitrite reductases (CuNiRs) have been isolated and characterized from a number of bacterial sources, including *Alcaligenes faecalis S-6* (*Af*NiR) (*2*), *Alcaligenes xylosoxidans* (*Ax*NiR) (*3*, *4*), *Achromobacter cycloclastes* (*Ac*NiR) (*5*), and *Pseudomonas aureofaciens* (*Pa*NiR) (*6*). CuNiRs are classified as either blue (*Ax*NiR and *Pa*NiR) or green (*Af*NiR and *Ac*NiR) based on their visible absorption spectra. X-ray crystallographic structures have been determined for the green NiRs from *Ac*NiR (*7*, *8*) and *Af*NiR (*9*, *10*) and the blue NiR from *Ax*NiR (*11*−*13*). The crystal structures show that they are all structurally similar, a trimer with each monomer or subunit consisting of two domains with a characteristic β-sandwich motif. Each monomer contains a buried type-1 Cu (T1Cu) site and a type-2 Cu (T2Cu) site at the interface between two monomers where the T2Cu ligands are provided by two adjacent monomers. The T1Cu site accepts electrons from an azurin/pseudoazurin, which are transferred to the T2Cu site where nitrite reduction occurs. The T1Cu ligand His139 is located at the bottom of

[†] This work was supported by the BBSRC/EPSRC's Biomolecular Sciences program (Grant number 719/B14224 to S.S.H.).

[‡] PDB accession codes are as follows 1WA0 (W138H), 1WA1 (H313Q), and 1WA2 (H313Q−NO_2).

* To whom correspondence should be addressed: Molecular Biophysics Group, CCLRC Daresbury Laboratory, Warrington, WA4 4AD, Cheshire, U.K. E-mail: s.hasnain@dl.ac.uk. Telephone: (44) 1925 603273. Fax: (44) 1925 603748.

[§] De Montfort University.

[||] CCLRC Daresbury Laboratory.

[⊥] Biological Chemistry Department, John Innes Centre.

[#] Molecular Microbiology Department, John Innes Centre.

[1] Abbreviations: *Ac*NiR, *Achromobacter cycloclastes* nitrite reductase; *Af*NiR, *Alcaligenes faecalis* nitrite reductase; *Ax*NiR, *Alcaligenes xylosoxidans* nitrite reductase; CuNiR, copper nitrite reductase; ENDOR, electron nuclear double-resonance spectroscopy; MES, 2-morpholinoethanesulfonic acid; NiR, dissimilatory nitrite reductase; *Pa*NiR, *Pseudomonas aureofaciens* nitrite reductase; PEG, poly(ethylene glycol); PEG−MME, poly(ethylene glycol)−monomethyl ether; rms, root mean square; SDS−PAGE, sodium dodecyl sulphate−polyacrylamide gel electrophoresis; SRS, Synchrotron Radiation Source; XAFS, X-ray absorption fine structure.

10.1021/bi048682g CCC: $27.50
Published on Web 12/03/2004

a small depression although it is orientated such that the $N^{\epsilon 2}$ atom is solvent-exposed. Located at the top of the depression are the residues Met87, Pro88, Met135, and Trp138. An ordered mechanism has been proposed for CuNiRs (*14*) where nitrite binds to the oxidized T2Cu site displacing a coordinated water molecule and then the T2Cu site is reduced via electron transfer from the T1Cu site. Recent electron-donation studies from Murphy and co-workers (*15*) have demonstrated that pseudoazurin can donate electrons readily to both green and blue CuNiRs, whereas azurin donates poorly to the green CuNiRs. A putative docking model of *Ax*NiR and *Ax* azurin-II was proposed, which results in a Cu−Cu distance of ~20 Å between NiR and azurin. This model positioned Tyr197 near the putative azurin-docking site, hence suggesting a possible electron-transfer route to the Cu ligand His139 via residue Trp138, which resides near the side chain of Tyr197. Trp138 is fully conserved in all of the known copper nitrite reductases and adopts an identical position structurally in all of the Cu nitrite reductases for which a crystal structure exist.

The nature of substrate binding in CuNiRs has been the focus of a number of spectroscopic and structural studies. Earlier electron nuclear double-resonance spectroscopy (ENDOR) (*16*) studies demonstrated that in oxidized nitrite-bound *Ax*NiR, the nitrite molecule binds O-coordinate. X-ray absorption fine structure (XAFS) studies from Strange et al. (*17*) confirmed this method of binding with a Cu−O distance of 1.98 Å, concomitant with an expansion of the Cu-coordination sphere and the change in coordination number on the binding of nitrite. Crystallographic studies have also shown that in nitrite-soaked green *Ac*NiR (*8*) the nitrite binds to the T2Cu in a bidentate fashion with Cu−O distances of ~2.2 and 2.5 Å. The crystal structure of nitrite-soaked *Ax*NiR (*11*) at 2.8 Å reported a bidentate mode of binding with Cu−O distances of ~1.7 and 2.4 Å. A high-resolution crystal structure of nitrite-soaked *Ax*NiR has not been possible to obtain because of the blocking of the "hydrophobic pocket" by extraneous poly(ethylene glycol) (PEG) from the crystallization solution via an interaction with His313, thus preventing access of the nitrite substrate to the active site. The pocket is lined by hydrophobic residues with two polar residues Glu133 and His313 at its opening. Glu133 is fully conserved among the blue and green CuNiRs, as is the His313 residue except in the blue *Pa*NiR, where the histidine is replaced by a glutamine.

We have determined the crystal structures of the *Ax*NiR Trp138His (1.6 Å resolution) and His313Gln (1.65 Å resolution) mutants, as well as the nitrite-soaked His313Gln−NO_2^- (1.72 Å) complex. The Trp138His mutant has near-full enzymatic activity compared to the native protein using methyl viologen (MV) as the electron donor but has a much reduced activity (~10%) when the physiological redox partner, azurin, is used. This suggests that Trp138 plays a significant role in the productive interaction between *Ax*NiR and azurin. The His313Gln mutant exhibits near-full activity with MV and reduced azurin I. The structures of this mutant and of its nitrite-bound complex confirm the role of the hydrophobic pocket in terms of the port of entry for the substrate.

EXPERIMENTAL PROCEDURES

Site-Directed Mutagenesis of the nirA Gene. Site-directed mutagenesis of the *nirA* gene in plasmid vector pEnirsp-1 was performed with the QuikChange Site-Directed Mutagenesis Kit (Stratagene). The oligonucleotides used to construct the *nirA* gene mutants for Trp138His were W138H-F(5′-GGCATGGTGCCCCATCACGTGGTGTCGG-3′), and W138H-R(5′-CCGACACCACGTGATGGGGCACCATGCC-3′), and for His313Gln, the oligonucleotides were H313Q-F(5′-GCGCCGCCGGCCAAATCAAGGTCGAGG-3′) and H313Q-R(5′-CCTCGACCTTGATTTGGCCGGCGGCGC-3′). The resulting plasmids were termed pEnirW138H and pEnirH313Q, which encoded the NiR mutants Trp138His and His313Gln, respectively. The complete DNA sequences of the mutant *nirA* genes were verified using the method of Sanger et al. (*18*).

Bacterial Growth and Enzyme Purification. The Trp138His and His313Gln mutant forms of *Ax*NiR were purified from periplasmic extracts of recombinant *Escherichia coli* cells as described previously Prudêncio et al. (*19*). The periplasmic fractions including the mutant proteins were dialyzed against 1 mM $CuSO_4$. Gel electrophoresis [sodium dodecyl sulphate−polyacrylamide gel electrophoresis (SDS−PAGE)] was used routinely to assess the purity of the protein samples. For pure preparations of NiR, the protein concentration was estimated using an extinction coefficient at 280 nm of 1.54 M^{-1} cm^{-1} (Eady, R., unpublished results).

Enzyme Activity Assays. NiR activity was determined using the discontinuous MV assay as described by MacGregor (*20*) and Abraham et al. (*3*). The reaction mixture contained in a final volume of 2 mL, 250 mM potassium phosphate buffer (pH 7.1), and 0.1 mM sodium nitrite. MV at a concentration of 0.5 mg mL^{-1} was used as the electron donor, and the reaction was initiated by the addition of dithionite to a final concentration of 0.4 mg mL^{-1} followed by gentle mixing. The mixture was then incubated at 25 °C for 5 min, and the reaction was stopped by vortexing to oxidize the residual dithionite. The amount of nitrite left in the mixture was then determined via the UV−vis spectra. One unit of enzyme activity is defined as the reduction of 1 μmol of nitrite per minute per milligram of protein.

In the case of the electron-donation experiments using the physiological redox partner, both reduced azurin I and NiR were checked for protein purity and were subsequently manipulated anaerobically in a glovebox. Sodium dithionite was added to a final concentration of 1 mM to a ~0.7 mM solution of azurin I in 1 mL of 50 mM 2-morpholinoethanesulfonic acid (MES) at pH 6.0. After incubation for 2 min, excess reductant was removed by passage of the protein through a Bio-Gel P-6 Desalting Gel (Bio-Rad) column (14 × 1 cm) equilibrated with degassed 100 mM Tris-HCl buffer at pH 7.1 and a flow rate of ca. 0.75 mL min^{-1}. After reduction and removal of the excess dithionite, azurin I had a concentration of ~0.45 mM in a total volume of ~1.5 mL. The activity assay measured the reoxidation of reduced azurin from the increase in absorption at 619 nm. The degassed reaction mixture contained either 150 or 70 μM reduced azurin I and 20 mM sodium nitrite in 100 mM Tris-HCl at pH 7.1. The reaction was performed under argon and was started by the injection of the NiR through the rubber closure of the cuvette. Oxidation of azurin I in the absence of the

Table 1: Summary of X-ray Data and Model Parameters

data quality	Trp138His	His313Gln	His313Gln−NO_2^-
space group	*H*3	*H*3	*H*3
resolution (Å)	1.60	1.65	1.72
unit cell (Å)	$a = b = 89.8$, $c = 143.5$	$a = b = 90.2$, $c = 143.7$	$a = b = 89.6$, $c = 143.6$
observed reflections	279 010	349 205	312 543
unique reflections	56 925	51 930	44 676
completeness (%)	95.6 (80.7)	98.5 (97.2)	97.5 (98.4)
R_{merge} (%)	4.5 (42.7)	9.2 (36.6)	9.1 (41.6)
$I/\sigma(I)$	22.4 (2.4)	8.5 (2.3)	8.7 (3.0)
R_{work} (%)	16.5	16.5	18.0
R_{free} (%)	19.2	19.3	21.0
model quality			
B factors			
Wilson (Å^2)	19.6	19.0	18.8
protein (Å^2)	21.8	19.3	22.3
water (Å^2)	34.5	28.2	31.4
ESU	0.07	0.07	0.09
B factor ESU based on ML	1.32	1.43	1.87
rms deviations			
bond distances (Å)	0.014	0.014	0.012
bond angles (deg)	1.49	1.54	1.44
Ramachandran plot (non-Gly and non-Pro)			
residues in most favored regions (%)	88.4	88.4	90.1
residues in additionally allowed regions (%)	11.2	11.2	9.5
residues generously allowed	0.4	0.4	0.4

enzyme was determined in a blank assay using water instead of a protein solution, and this slope was subtracted from the one obtained for the protein assays.

In assays designed to test the effect of PEG as an inhibitor, 70 μM reduced azurin I was used as an electron donor in the presence of 10% PEG with precipitant conditions used for crystallization. Higher concentrations of PEG have not been used because it is likely to prevent interaction between azurin and NiR. Dithionite could not be used as an electron donor because of the high nonenzymic rate of oxidation observed in the presence of PEG and nitrite.

Protein Crystallization. Crystals of Trp138His and His313Gln NiR were grown by the hanging-drop vapor diffusion method at 21 °C. A total of 2 μL of 6−8 mg mL^{-1} protein in 10 mM Tris-HCl at pH 7.1 was mixed with an equal volume of reservoir solution consisting of 25% PEG−monomethyl ether (MME) 550, 10 mM zinc sulfate, and 0.1 M MES at pH 6.5 and suspended over a 500 μL reservoir. Crystals of both mutants were an intense blue color and grew within 2 days to the approximate dimensions 0.9 × 0.6 × 0.1 mm in a rhombohedral morphology. For His313Gln−NO_2^-, 10 mM sodium nitrite was added to the reservoir solution prior to crystallization.

Data Collection, Structure Solution, and Refinement. Crystals were transferred from their drops into a cryostream using cryo-loops and then flash-cooled to 100 K. The reservoir solution served as an effective cryoprotectant. Data were collected using an ADSC Quantum-4 CCD detector on station 14.1 at the Synchrotron Radiation Source (SRS), Daresbury Laboratory, at an X-ray wavelength of 1.48 Å. Data were scaled and merged in HKL2000 (*21*). The structures were solved using the molecular replacement method implemented in AMoRe (*22*) using native *Ax*NiR (PDB accession code 1OE1) as the search model. The structures were refined using the maximum-likelihood method with a bulk solvent correction as implemented in REFMAC5 (*23*) and rebuilt interactively using "O" (*24*). A test set of reflections comprising 5% were set aside for calculation of the cross-validation free *R* factor (*25*). During the refinement protocol, no restraints were applied to the metal−ligand bond distances or angles. Solvent molecules were added using ARP/wARP (*26*). Residues 1 and 336 (the N and C termini) were poorly defined in the electron density and therefore were set to zero occupancy. Several Zn atoms were modeled at the protein surface. The heterocompounds MES and PEG (tetraethylene glycol, 4 repeating units) were added to the models on the basis of the shape and difference density peaks in the $2F_o - F_c$ and $F_o - F_c$ density maps. In the case of His313Gln−NO_2^-, the nitrite molecule was built into clear $2F_o - F_c$ and $F_o - F_c$ electron density following examination of the maps. The final *R* factors for Trp138His, His313Gln, and His313Gln−NO_2^- were 16.5% (R_{free} = 19.2%). 16.5% (R_{free} = 19.3%), and 18.0% (R_{free} = 21.0%), respectively. Refinement statistics for the structures are summarized in Table 1.

RESULTS AND DISCUSSION

Enzyme Activity Measurements. The catalytic activities of the Trp138His and His313Gln mutants were measured by two methods using either an artificial electron donor (reduced MV) or the physiological electron donor to *Ax*NiR, reduced azurin I from *A. xylosoxidans*. Fully Cu-loaded recombinant native *Ax*NiR was used as a control. In the electron-donation experiments, a 100−250-fold excess of reduced azurin I over the T1Cu center of *Ax*NiR was used. With the artificial electron donor, both Trp138His and His313Gln exhibited near-full activity of native NiR [260 μmol of MV reoxidized min^{-1} (mg^{-1} of protein)]. In the azurin assay system, reduced azurin I was used as the electron donor. The activity for His313Gln was ∼80% of the activity observed for native NiR, whereas the Trp138His mutant had a much reduced activity of ∼10% that of the native *Ax*NiR protein. The time course of azurin assays of NiR, His313Gln, and Trp138His using reduced azurin (70 μM) and 95 nM NiR (i.e., 285 nM T1Cu site of NiR) are shown in Figure 1. The nonlinearity of the curves for native and H313Q has been observed

Table 2: Cu−Ligand Distances at the T1Cu and T2Cu Sites

atom 1	atom 2	1.04 Å resolution[a] [native (Å)]	Trp138His (Å)	His313Gln (Å)	His313Gln−NO_2^- (Å)
T1Cu	His89 $N^{\delta 1}$	2.02	2.10	2.10	2.11
T1Cu	Cys130 S^{δ}	2.20	2.12	2.16	2.13
T1Cu	His139 $N^{\delta 1}$	2.03	2.10	2.04	2.05
T1Cu	Met144 S^{δ}	2.45/4.26	2.63	2.60	2.56
T2Cu	His94 $N^{\epsilon 2}$	1.96	2.02	2.04	2.01
T2Cu	His129 $N^{\epsilon 2}$	2.00	2.02	1.99	2.05
T2Cu	HisB249 $N^{\epsilon 2}$	3.74	3.93	4.01	3.93
T2Cu	HisB300 $N^{\epsilon 2}$	2.00	2.08	2.07	2.13
T2Cu	Wat503	1.98	2.06	2.00	
Wat503	Asp92 $O^{\delta 2}$	2.54	2.51	2.55	
Wat600	Asp92 $O^{\delta 1}$	2.88	2.72	2.89	2.80

previously and arises from the formation of the inhibitory dead-end complex of NiR (*15*). In comparing rates, the initial rates were calculated from the first 2 min of the reaction curves. The low rate of donation from Trp138His, Figure 1c, indicates that this mutation has a marked effect on the ability of azurin to support NiR activity. In this case, the curvature discussed above is not seen, suggesting that the mutation impedes the formation of such complexes on these time scales. The activity increased by only 8% when the azurin concentration was increased from 70 to 150 μM. Thus, the low rate observed for the Trp138His mutant is not a consequence of an increased apparent K_m. The very slow reaction rate made determination of the apparent K_m experimentally inaccessible because increasing [NiR] obtains higher rates, while decreasing [azurin] to nonsaturating levels rapidly leads to a situation where the [T1Cu site] approaches that of [azurin]. The observation that both the T1Cu and T2Cu sites are intact in Trp138His and that the activity using an artificial electron donor (which would not be limited by the need for protein-complex formation prior to electron transfer) was close to full activity, strongly suggests that the mutation of Trp138 to histidine has a significant effect on the productive complex formation with the physiological partner protein azurin I. Because the low rate is not due to an effect of saturation of NiR with azurin we propose that the mutation Trp138His results in a slower electron-transfer rate between azurin and the T1Cu center of NiR.

Quality of the Models and Overall Structure. The structures of Trp138His, His313Gln, and nitrite-bound His313Gln (His313Gln−NO_2^-) have been refined to *R* factors of 0.165, 0.165, and 0.180, respectively (R_{free} = 0.192, 0.193, and 0.210). Each structure has a number of heteroatoms (sulfate and MES). Residues 1 and 336 were set to zero occupancy owing to the lack of electron density, while residues 2−7 at the N termini have relatively high main-chain *B* factors (>45 Å^2), with a similar pattern observed at the C termini. Quality indicators for the structures are given in Table 1. The mutants retain the typical trimeric structure observed in native *Ax*NiR. A superposition of the Cα atoms of the structures [superposition of equivalent monomers by LSQMAN (*27*)] with those of the native protein (*13*) shows a root-mean-square (rms) deviation of 0.29 Å for the Trp138His structure and 0.26 Å for the His313Gln structure. Significant structural differences are generally limited to the immediate mutation sites and the N and C termini, which show a significant level of disorder. This disorder is typical of NiR structures determined in space group *H*3 (our unpublished results). If residues 1−7 and 336 are omitted from the superposition, the rms deviations in Cα positions are reduced to 0.22 and 0.25 Å, respectively. The rms difference in Cα positions between His313Gln and His313Gln−NO_2^- is just 0.10 Å. For comparison, the ESU for the structures is 0.07−0.09 Å (Table 1).

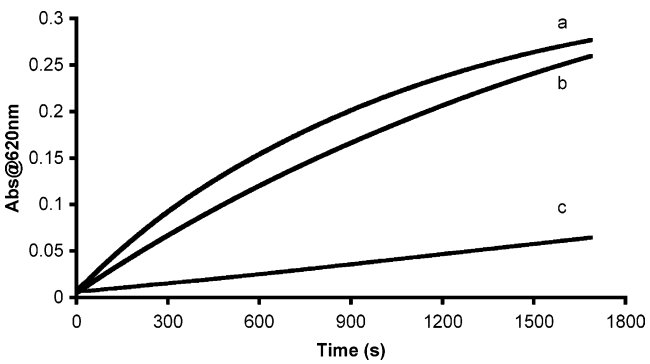

FIGURE 1: Time course for azurin oxidation for (a) native AxNiR, (b) H313Q, and (c) W138H.

Copper Sites and Water Networks. A comparison of the T1Cu sites with those in native NiR (*13*) shows little change (Table 2). In all of the structures, the temperature factor of the Cu ion is comparable to that of the surrounding ligands, indicating that a full complement of Cu is present. Prior to crystal growth the 280:595 nm absorption ratio was determined to be less than 10 for both Trp138His and His313Gln. Such a ratio is indicative of a full occupancy of the T1Cu center. Electron paramagnetic resonance (EPR) data for both mutants (data not shown) confirms that both a T1Cu and T2Cu center are present. The superposition of the T1Cu site in His313Gln and His313Gln−NO_2^- shows that they are essentially identical. In the Trp138His structure, a small rotation (∼20°) of the imidazole ring of His139 is observed, although the position of the Cu is unchanged. A comparison of the T2Cu sites in the mutant structures with that of native *Ax*NIR shows that the position of the Cu ligands His129, His300, and Asp92 is unchanged in the mutants. A comparison of the Cu−ligand bond distances in Trp138His and His313Gln with the native protein is given in Table 2. There is, however, some change in the position of the Cu atom and water molecules as well as an increase of some 0.2−0.25 Å in the HisB249−Cu bond length (the T2Cu ligand His249 originates in an adjacent monomer and is therefore referred to as HisB249). This is due to a very small rotation in the imidazole ring of HisB249 relative to its position in native *Ax*NiR.

It has been previously proposed (*12*, *28*) that the protons required for the reduction of nitrite in the catalytic mechanism are delivered to the T2Cu site via a highly ordered water network. In addition a so-called "secondary" water network

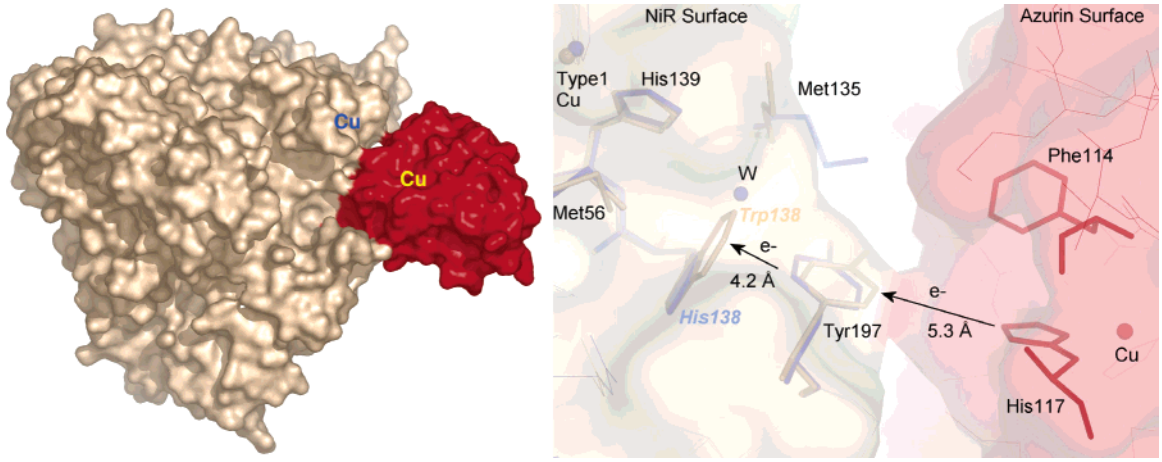

FIGURE 2: (Left) Docking model of nitrite reductase (light brown) with azurin II (red) (*15*). (Right) Superposition of Trp138His (orange) and native *Ax*NiR (blue) in the vicinity of the mutation site. The histidine imidazole occupies a near-identical position to the first ring of Trp138. The position of Tyr197, implicated in complex formation, is subtly altered, and its O atom forms a 2.7 Å bond to the S atom of Met135, which adopts a different rotamer to that in native *Ax*NiR. Also shown is the position of residues from the azurin molecule from theoretical docking calculations (red).

was proposed (*29*), although this was only observed in the structures determined at higher pH. However, the atomic resolution structure of native *Ax*NiR (*13*) was determined at pH 6.5 and revealed that both the primary and secondary water networks were present and well-defined. In the structures presented here (determined at pH 6.5), both of these water networks are also well-defined and essentially unchanged from that present in native *Ax*NiR determined at atomic resolution (*13*).

Trp138His Mutation Site. The orientation of the side chain of His138 is such that its imidazole ring superimposes closely with the position of the "first ring" of Trp138 in native *Ax*NiR, Figure 2. In the Trp138His structure, an additional water molecule is present, hydrogen-bonded at a distance of 2.7 Å to His138. This water also makes a weak (3.5 Å) bond with the $N^{\epsilon 1}$ atom of His139. The side chain of His138 is ~3.2 Å distant from that of Tyr197, which adopts a new conformation. The separation of the His138 and His139 side chains is ~4.6 Å. The residues in the vicinity of His138 show several structural changes in the mutant structure. The principal differences involve residues Tyr197 and Met135. Tyr197 shows both a lateral shift and slight rotation of its side chain in comparison with its position in native *Ax*NiR. This results in a shift in the position of its side-chain oxygen atom of around 1.4 Å relative to the native protein. The shift appears to be due to the removal of the close steric contact from the side chain of Trp138. The flexible side chain of Met135 occupies a different rotamer in the Trp138His mutant, although it is not clear from the structure why this is the case. The sulfur atom of Met135 is now located at only 3.25 Å from the terminal oxygen atom of Tyr197, in comparison with more than 6 Å in the native structure.

Implications for Electron Transfer. The T1Cu site of *Ax*NiR lies at the base of a depression in the protein surface, presenting the Nϵ2 atom of the Cu−ligand His139 toward the solvent. Electron transfer from the physiological electron-donor protein, azurin, to T1Cu in *Ax*NiR is thought to occur via His139. In the docking model of *Ax*NiR and azurin II (*15*, Figure 2), Tyr197 is identified as a key residue at the intermolecular interface and could receive an electron from the solvent-exposed Cu ligand His117 of azurin (these residues are ~5 Å apart in the docking model). Residue Trp138 lies between His139 and Tyr197 and is therefore likely to play a role in electron transfer between azurin and the T1Cu site of NiR by linking the potential azurin-docking site to the T1Cu ligand His139. The plane of the side chain of Trp138 is approximately perpendicular to that of Tyr197 and ~3.5 Å distant (Figure 2). Because residues 138 and 197 are distant in the amino acid sequence, it is probable that the first step of the intramolecular electron transfer pathway occurs via a through-space process between these two aromatic side chains. Amino acids containing aromatic rings as part of their side chains (Trp, Tyr, and Phe) are well-suited to act as intermediaries in electron transfer because the delocalized electron systems in the aromatic rings may act both as electron donors and acceptors. Through-space electron transfer between tyrosine and tryptophan residues has been the subject of a recent theoretical study (*30*). Subsequent electron transfer from Trp138 to His139 and hence to T1Cu is most likely to occur via a covalent pathway along the protein main chain connecting these two residues or, less probably, via a second through-space transfer to the His139 side chain, which is ~3.5 Å away from that of Trp138. From His139, the electron is transferred to copper, producing the Cu^{I} site required for subsequent electron transfer to the catalytic T2Cu site.

There are several notable features of the crystal structure of the Trp138His mutant that could contribute to the observed reduction in activity of this mutant compared to the native protein. First, through-space electron transfer from Tyr197 to His138 would be expected to be less efficient than the Tyr197 to Trp138 interaction, even though the shift in the position of Tyr197 in the mutant structure results in a slightly closer approach of the two residues. Tryptophan is generally regarded as the most effective intermediate residue in electron-transfer pathways because of the number of delocalized π electrons in its double-ring aromatic side chain. Additionally, the presence of a water molecule hydrogen-bonded to the Nϵ2 atoms of both His138 and His139 may impose additional limits to an efficient electron transfer. In the native protein, this water position is sterically excluded by the presence of the bulky tryptophan side chain. Second,

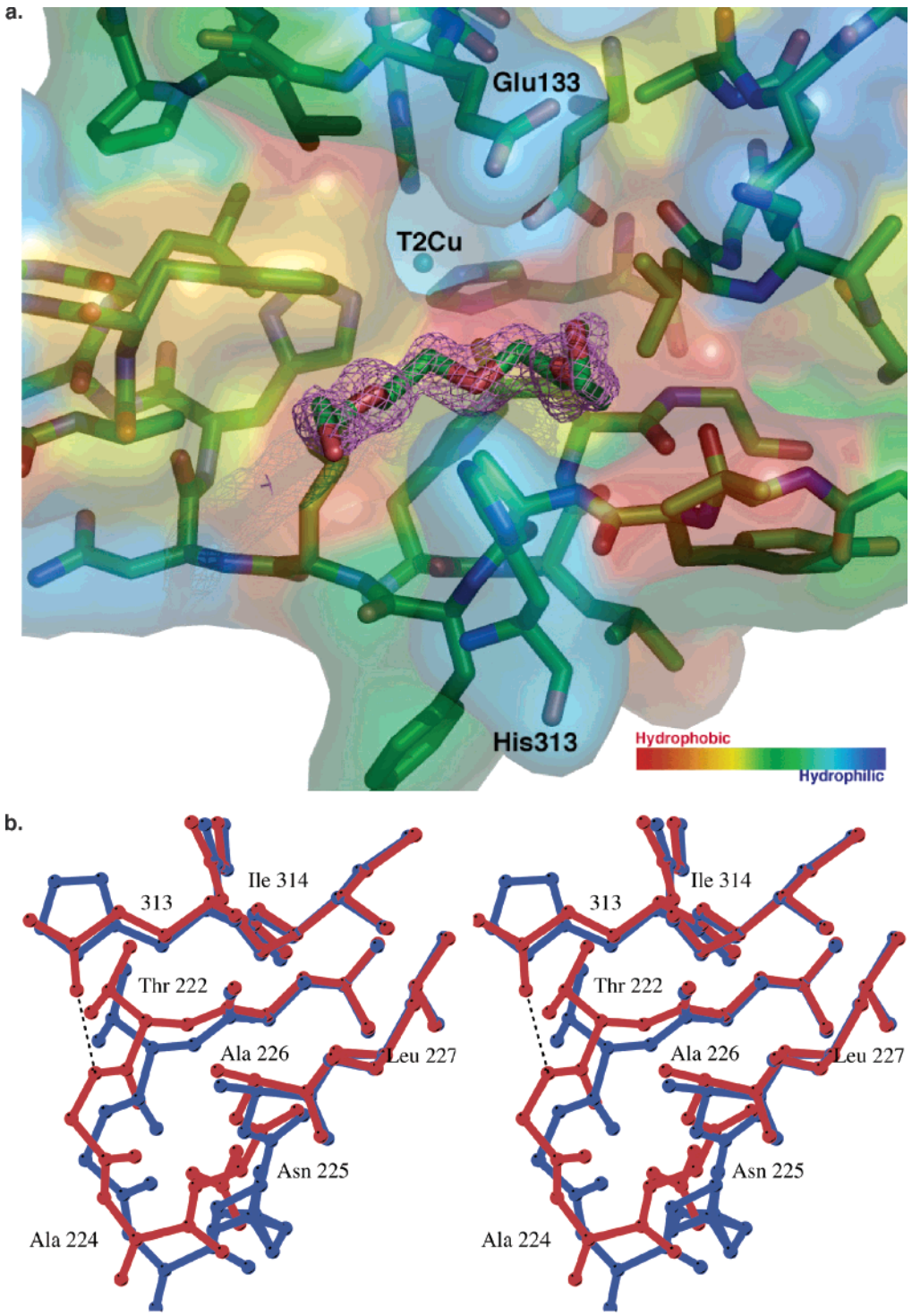

FIGURE 3: (a) View of the hydrophobic pocket in Trp138His illustrating the $2F_o - F_c$ electron density contoured at 1σ for the PEG molecule, which plugs the opening of the pocket by hydrogen bonding to His313. The hydrophobic surface is also displayed and is colored by hydrophobicity. (b) Stereo cartoon of the superposition of His313Gln and native NiR at the mutation site. The glutamine side chain forms a hydrogen bond to the backbone of residue Gly223, which forces a change in the conformation of the loop region from Thr222 to Ala226.

the small observed shift in the position of Tyr197 away from the protein surface and its new interaction with Met135 could diminish the efficiency of electron transfer to tyrosine from the surface-exposed histidine of azurin. It must be noted however, that the theoretical docking analysis treated both the *Ax*NiR and azurin molecules as rigid bodies, and the likely conformational changes as a result of the protein−protein interactions have not been considered. A full understanding of the electron-transfer pathway between *Ax*NiR and azurin must await a structure determination of their protein−protein complex, which despite much effort by several groups working with several different NiRs, has remained elusive.

His313Gln Mutation Site and Nitrite Binding. The so-called "hydrophobic patch" on the surface of *Ax*NiR has previously been suggested as the entry point through which nitrite reaches the T2Cu site. The crystal structure of Trp138His reveals that PEG is bound to His313 and is

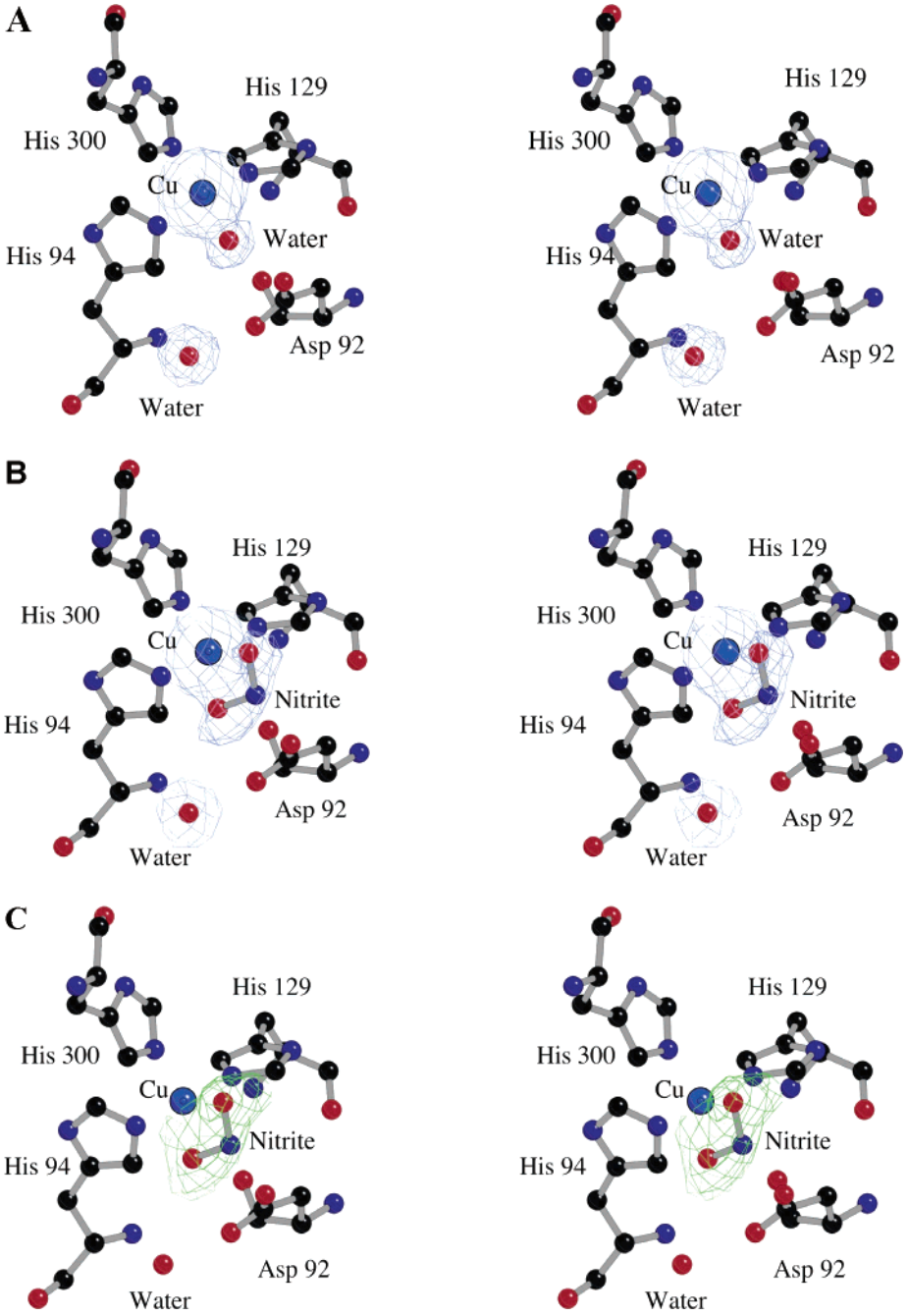

FIGURE 4: (A) Stereo $2F_o - F_c$ electron density contoured at 1σ showing the ordered water molecule ligating the T2Cu site in His313Gln. Density for the water molecule that ligates the Asp92 side chain is also shown for comparison. (B) Stereo $2F_o - F_c$ electron density contoured at 1σ for the T2Cu site of His313Gln$-NO_2^-$. (C) $F_o - F_c$ omit map contoured at 3σ showing the nitrite molecule.

plugging the pocket in a manner similar to that seen in the native protein (*13*) (Figure 3a). Previous nitrite-soaking experiments on native *Ax*NiR and several mutants of *Ax*NiR using crystals grown in the presence of PEG as a precipitant have proved to be unsuccessful. This observation gave further support to the hypothesis that the hydrophobic pocket is in fact the port of entry for the nitrite substrate.

The His313Gln mutation eliminates this interaction with exogenous PEG, thus, allowing the substrate to enter. In this mutant, Gln313O$^{\epsilon 1}$ forms a 2.95 Å hydrogen bond to the amide nitrogen of Gly233, while the N$^{\epsilon 1}$ atom of Gln313 is oriented toward the entry of the hydrophobic patch. This new hydrogen-bond interaction forces the short loop region between residues 221 and 226 to adopt a new conformation (Figure 3b) and results in the glutamine side chain having a lower mobility than the histidine that it replaces, as well as occupying a smaller volume.

$2F_o - F_c$ electron density maps contoured at 1σ for the T2Cu sites in His313Gln and His313Gln$-NO_2^-$ are shown in parts a and b of Figure 4. In His313Gln, the ligating water molecule at the T2Cu is clearly evident in the electron density with a uniform shape indicative of a well-ordered water molecule. This is reflected in the *B* factor of the water at 21 Å^2. In contrast, the elongated bifurcated electron density observed in Figure 4b is consistent with the presence of a nitrite molecule at the T2Cu site in this structure. On the basis of the *B* factors of its ligating atoms, the nitrite occupancy was estimated at 0.5. An $F_o - F_c$ omit map for the nitrite molecule contoured at 3σ is shown in Figure 4c confirming the presence of nitrite. The mode of nitrite

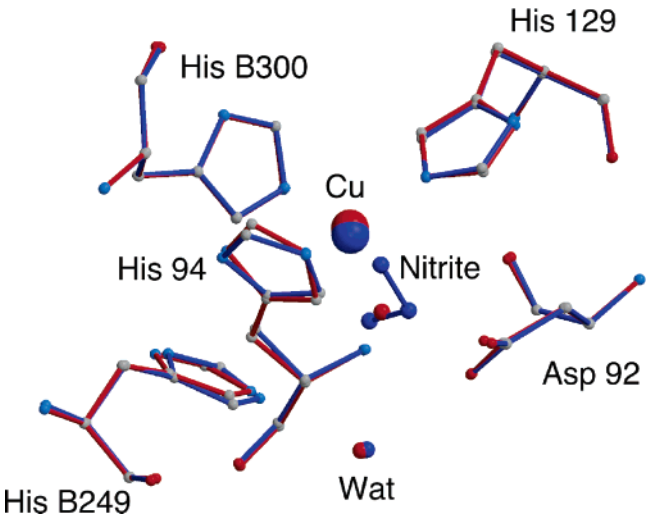

FIGURE 5: Superposition of the His313Gln−NO_2^- structure (blue) with the His313Gln structure (red). The O1 atom of the nitrite is shifted some 0.5 Å in comparison to the water ligating the Cu in the native protein. The largest rearrangement in Cu geometry is the rotation of the ring of HisB249.

binding is consistent with that observed in the green *Ac*NiR with oxygen−Cu distances of ∼1.9 and ∼2.4 Å for nitrite O1 and O2, respectively. The O1 atom of nitrite is hydrogen-bonded to Asp92$O^{\delta 2}$ at ∼2.7 Å and to His94$N^{\epsilon 1}$ at ∼2.7 Å. The O2 atom forms hydrogen bonds to both HisB300 at ∼2.4 Å and HisB249 at ∼2.8 Å. A superposition of His313Gln−NO_2^- with His313Gln is shown in Figure 5. Both His94 and HisB249 show small shifts in their orientations on nitrite binding.

His313Gln Mutation and Effect of PEG on Activity. The binding site for PEG over the hydrophobic patch that prevents access of nitrite to the T2 center in crystals of native *Ax*NiR suggests that PEG should inhibit activity and that the His313Gln mutation should, in view of the above structural results, alleviate inhibition. To confirm this, assays with and without 10% PEG were performed for the native and mutant enzymes. The His313Gln showed 17% reduction compared to 63% inhibition for the wild type. The small reduction in activity for H313Gln may partly be due to perturbation of the azurin binding to NiR arising from the increased viscosity because of PEG. These findings provide confirmation that nitrite channelling involves this pocket.

CONCLUSIONS

The mutation of tryptophan 138 to histidine has little effect on the overall structure of nitrite reductase, with both Cu sites and the proton channels remaining intact. It is therefore intriguing to observe contrasting enzymatic activity results using an artificial (MV) donor and the physiological electron donor, azurin I. Our data show that the mutation disrupts a likely route of electron transfer from residue Trp197, located at the molecular surface and proposed to play a role in complex formation with azurin, to the T1Cu ligand His139 via the mutated residue Trp138. This suggests that the highly conserved Trp138 residue is a key participant in electron transfer from the physiological partner. The mutation of His313 to Gln causes a change in the conformation of the loop region from Thr222 to Ala226 because of the hydrogen bonding of Gln313 to the backbone of Gly223. In addition, the His313Gln mutation has prevented the previously observed binding of PEG in a position to block the hydrophobic pocket, thus, allowing entry of the substrate to the T2Cu center and confirming that His313 is the port of substrate entry. Nitrite binds to Cu in an O-coordinate, asymmetric bidentate manner and is orientated such that the nonligating HisB249 is in a position to anchor the substrate along with Asp92. The high-resolution structural results together with the activity data in the presence and absence of PEG establishes that His313 is located at the port of substrate entry.

ACKNOWLEDGMENT

The authors thank CCLRC and BBSRC for provision of facilities at Daresbury Laboratory and the John Innes Centre, respectively. The work was supported by a BBSRC Grant, B14224, to S.S.H. The figures were created using Pymol (*31*), Molscript (*32*), Bobscript (*33*), and Raster3D (*34*).

REFERENCES

1. Eady, R. R., and Hasnain, S. S. (2003) Denitrification, *Compr. Coord. Chem. II 8*, 759−786.
2. Kakutani, T., Watanabe, H., Arima, K., and Beppu, T. (1981) Purification and properties of a copper-containing nitrite reductase from a denitrifying bacterium, *Alcaligenes faecalis*, *J. Biochem. 89*, 453−461.
3. Abraham, Z. H., Lowe, D. J., and Smith, B. E. (1993) Purification and characterisation of the dissimilatory nitrite reductase from *Alcaligenes xylosoxidans* subsp. *xylosoxidans* (NCIMB 11015): Evidence for the presence of both type 1 and type 2 copper centres, *Biochem. J. 295*, 587−593.
4. Masuko, M., Iwasaki, H., Sakurai, T., Suzuki, S., and Nakahara, A. (1984) Characterization of nitrite reductase from a denitrifier, *Alcaligenes* sp. NCIB 11015. A novel copper protein, *J. Biochem. 96*, 447−454.
5. Iwasaki, H., and Matsubara, T. (1972) A nitrite reductase from *Achromobacter cycloclastes*, *J. Biochem. 71*, 645−652.
6. Zumft, W. G., Gotzmann, D. J., and Kroneck, P. M. (1987) Type 1, blue copper proteins constitute a respiratory nitrite-reducing system in *Pseudomonas aureofaciens*, *Eur. J. Biochem. 168*, 301−307.
7. Godden, J. W., Turley, S., Teller, D. C., Adman, E. T., Liu, M. Y., Payne, W. J., and LeGall, J. (1991) The 2.3 Å X-ray structure of nitrite reductase from *Achromobacter cycloclastes*, *Science 253*, 438−442.
8. Adman, E. T., Godden, J. E., and Turley, S. (1995) The structure of copper nitrite reductase from *Achromobactor cycloclastes* at 5 pH values, with NO_2^- bound, and with type-2 Cu^{II} depleted, *J. Biol. Chem. 270*, 27458−27474.
9. Kukimoto, M., Nishiyama, M., Murphy, M. E. P., Turley, S., Adman, E. T., Horinouchi, S., and Beppu, T. (1994) X-ray structure and site directed mutagenesis of a nitrite reductase from *Alcaligenes faecalis*-S6−Roles of 2 copper atoms in nitrite reduction, *Biochemistry 33*, 5246−5252.
10. Murphy, M. E. P., Turley, S., Kukimoto, M., Nishiyama, M., Horinouchi, S., Sasaki, H., Tanokura, M., and Adman, E. T. (1995) Structure of *Alcaligenes faecalis* nitrite reductase and a copper site mutant, M150E, that contains zinc, *Biochemistry 34*, 12107−12117.
11. Dodd, F. E., Hasnain, S. S., Abraham, Z. H. L., Eady, R. R., and Smith, B. E. (1997) Structures of a blue-copper nitrite reductase and its substrate bound complex, *Acta Crystallogr., Sect. D 53*, 406−418.
12. Dodd, F. E., van Beeumen, J., Eady, R. R., and Hasnain, S. S. (1998) X-ray structure of a blue-copper nitrite reductase in two crystal forms. The nature of the copper sites, mode of substrate binding, and recognition by redox partner, *J. Mol. Biol. 282*, 369−382.
13. Ellis, M. J., Dodd, F. E., Sawers, G., Eady, R. R., and Hasnain, S. S. (2003) Atomic resolution structures of native copper nitrite reductase from *Alcaligenes xylosoxidans* and the active site mutant Asp92Glu, *J. Mol. Biol. 328*, 429−438.

14. Strange, R. W., Murphy, L. M., Dodd, F. E., Abraham, Z. H. L., Eady, R. R., Smith, B. E., and Hasnain, S. S. (1999) Structural and kinetic evidence for an ordered mechanism of nitrite reductase, *J. Mol. Biol. 287*, 1001−1009.
15. Murphy, L. M., Dodd, F. E., Yousafzai, F. K., Eady, R. R., and Hasnain, S. S. (2002) Electron donation between copper containing nitrite reductases and cupredoxins: The nature of protein−protein interaction in complex formation, *J. Mol. Biol. 315*, 859−871.
16. Howes, B. D., Abraham, Z. H. L., Lowe, D. J., Brüser, T., Eady, R. R., and Smith, B. E. (1994) EPR and electron nuclear double resonance (ENDOR) studies show nitrite binding to the type 2 copper centres of the dissimilatory nitrite reductase of *Alcaligenes xylosoxidans*, *Biochemistry 33*, 3171−3177.
17. Strange, R. W., Dodd, F. E., Abraham, Z. H. L., Grossmann, J. G., Brüser, T., Eady, R. R., Smith, B. E., and Hasnain, S. S. (1995) The substrate binding site in Cu nitrite reductase and its similarity to Zn carbonic anhydrase, *Nat. Struct. Biol. 2*, 287−292.
18. Sanger, F., Nicklen, S., and Coulson, A. R. (1977) DNA sequencing with chain terminating inhibitors, *Proc. Nat. Acad. Sci. U.S.A. 74*, 5463−5467.
19. Prudencio, M., Eady, R. R., and Sawers, G. (1999) Catalytic and spectroscopic analysis of blue copper-containing nitrite reductase mutants altered in the environment of the type 2 copper centre: Implications for substrate interaction, *J. Bacteriol. 181*, 2323−2329.
20. MacGregor, C. H. (1978) Isolation and characterization of nitrate reductase from *Escherichia coli*, *Methods Enzymol. 53*, 347−355.
21. Otwinowski, Z., and Minor, W. (1997) Processing of X-ray diffraction data collected in oscillation mode, *Methods Enzymol. 276*, 307−326.
22. Navaza, J. (1994) AMoRe: An automated package for molecular replacement, *Acta Crystallogr., Sect. A 50*, 157−163.
23. Murshudov, G. N., Vagin, A. A., and Dodson, E. J. (1997) Refinement of macromolecular structures by the maximum likelihood method, *Acta Crystallogr., Sect. D 53*, 240−255.
24. Jones, T. A., Zou, J. Y., Cowan, S. W., and Kjeldgaard, M. (1991) Improved methods for building protein models in electron density maps and the location of errors in these models, *Acta Crystallogr., Sect. A 47*, 110−119.
25. Brünger, A. T. (1992) Free *R* value: A novel statistical quantity for assessing the accuracy of crystal structures, *Nature 355*, 472−475.
26. Lamzin, V. S., and Wilson, K. S. (1993) Automated refinement of protein models, *Acta Crystallogr., Sect. D 49*, 129−147.
27. Kleywegt, G. J. (1999) Experimental assessment of differences between related protein crystal structures, *Acta Crystallogr., Sect. D 55*, 1878−1857.
28. Ellis, M. J., Prudencio, M., Dodd, F. E., Strange, R. W., Sawers, G., Eady, R. R., and Hasnain, S. S. (2002) Biochemical and crystallographic studies of the Met144Ala, Asp92Asn, and His254Phe mutants of the nitrite reductase from *Alcaligenes xylosoxidans* provide insight into the enzyme mechanism, *J. Mol. Biol. 316*, 51−64.
29. Ellis, M. J., Dodd, F. E., Strange, R. W., Prudencio, M., Sawers, G., Eady, R. R., and Hasnain, S. S. (2001) X-ray structure of a blue copper nitrite reductase at high pH and in copper-free form at 1.9 Å resolution, *Acta Crystallogr., Sect. D 57*, 1110−1118.
30. Xiang-Yain, Li (2000) Electron transfer between tryptophan and tyrosine: Theoretical calculation of electron-transfer matrix element for intramolecular hole transfer, *J. Comp. Chem.* 22, 565−579.
31. DeLano, W. L. (2002) *The Pymol User's Manual* (DeLano, W., Ed.) DeLano Scientific, San Carlos, CA.
32. Kraulis, P. J. (1991) MOLSCRIPT: A program to produce both detailed and schematic plots of protein structures, *J. Appl. Crystallogr. 24*, 946−950.
33. Esnouf, R. M. (1997) An extensively modified version of MOLSCRIPT that includes greatly enhanced coloring capabilities, *J. Mol. Graphics Modell. 15*, 112−134.
34. Merritt, E. A., and Bacon, D. J. (1997) Raster3D: Photorealistic molecular graphics, *Methods Enzymol. 277*, 505−524.

BI048682G